LNF-96/042(P)

A New Non-Intercepting Beam Size Diagnostics Using Diffraction Radiation From a Slit

M. Castellano

Nuclear Instruments & Methods A 394, 275-280, (1997)

Nuclear Instruments and Methods in Physics Research A 394 (1997) 275–280

NUCLEAR INSTRUMENTS & METHODS IN PHYSICS RESEARCH Section A

A new non-intercepting beam size diagnostics using diffraction radiation from a slit

M. Castellano

INFN, Laboratori Nazionali di Frascati, P.O. BOX 13, 00044 Frascati, Italy

Received 16 September 1996

Abstract

A new non-intercepting beam size diagnostics for high-charge electron beams is presented. This diagnostics is based on the analysis of the angular distribution of the "diffracted" transition radiation emitted by the beam when crossing a slit cut in a metallic foil. It allows a resolution better than the radiation transverse formation zone. Numerical results based on the parameters of the TTF FEL beam are given as examples.

1. Introduction

The development of high-charge density electron beams is pursued in all major laboratories for at least two main objectives: high-energy electron–positron linear colliders and single pass X-ray free electron lasers.

In both cases, high-charge per pulse and low-emittance to reduce the transverse beam dimension are required. Emittance, on the other hand, may be increased by a rather large number of unwanted or uncontrolled effects: space charge, short-range and long-range wake fields, residual chromaticity and even the newly rediscovered tail–head radiative interaction in bending magnets [1].

The beam transverse dimension measurement is the simplest way to verify the corresponding to the project or to discover unwanted effects, but the high power density deposited by these beams in standard intercepting devices, like view screens, grids or scanning wires, make their use impossible unless with reduced current or shorter bunches. The development of new high-resolution, non-intercepting diagnostics for beam size measurement must therefore proceed together with that of the beams themselves.

In this paper, I will present the possibility of measuring the beam transverse dimension through the analysis of the angular distribution of the diffraction radiation emitted by the beam when crossing a slit cut in a conducting foil.

The measurement is fully non-intercepting, causing only a small perturbation to the beam, and is performed by means of a simple CCD camera.

As an extra bonus, this method, even if based on the detection of transition radiation, allows a resolution better than the transverse formation zone of this radiation, which is thought to be a limit, not yet experimentally verified, for beam spot resolution at high energy.

I will give numerical examples based on the parameters of the TESLA Test Facility (TTF) beam [2], which is a test bench for the TESLA Linear Collider, and on which the first experiments with this diagnostics will be performed. In particular, a single pass SASE Free Electron Laser experiment in the UV is scheduled on this accelerator [3], requiring a very low-emittance, high charge beam, for which a non-intercepting diagnostics is fundamental.

2. Diffraction radiation from a slit

Diffraction radiation is the radiation emitted by a charged relativistic particle going through an aperture in a metallic foil. If the aperture in the foil is larger than the beam transverse dimension, we have a real non-intercepting device, also giving only a small perturbation to the beam.

The mathematical derivation of diffraction radiation properties in different environment conditions is rather complex, but has been extensively studied [4–7]. In the accelerator physics, diffraction radiation plays an extremely important role as a source of beam energy losses, and has been studied principally for circular machines, with the main focus on the effects on the beam and not on the radiation itself.

Although in these studies the diffraction radiation has been considered as an independent form of radiation, it is

PII S0168-9002(97)00570-6

evident that it is nothing else than the transition radiation emitted by a surface with a cut on it which gives rise to a "diffraction" distribution.

The simplest cuts in a metallic foil are a round hole or a slit, but the latter must be preferred for a number of practical reasons: a fixed width slit can be moved to intercept the beam by means of a single linear actuator, while two half foils, independently moved along the same plane, allow to find the beam without intercepting it and also form a variable width slit.

For these reasons I will concentrate on the analysis of diffraction radiation from a slit, starting from the equations given in Ref. [7].

In a previous note [8], I have already shown the possibility to measure the bunch length through the analysis of the far infrared spectrum of the coherent diffraction radiation emitted by the same type of non-intercepting device. In this paper I will deal with radiation in the optical bandwidth, for which a large number of imaging instruments are available.

When an electron crosses, with normal incidence, a slit of width a symmetrically cut in a perfectly conducting foil around the x-axis, the angular distribution of emitted photons of wavelength λ in a bandwidth $d\lambda$, around both forward and backward directions, is given by

$$\frac{dN}{d\Omega} = -2\pi^2 \frac{k^2 c}{\hbar} \frac{d\lambda}{\lambda} \{|E_x|^2 + |E_y|^2\}, \tag{1}$$

with $k = 2\pi/\lambda$ and

$$E_x(k_x, k_y) = \frac{iek_x}{4\pi^2 cf}\left(\frac{e^{-(a/2-y)(f-ik_y)}}{f-ik_y} + \frac{e^{-(a/2+y)(f+ik_y)}}{f+ik_y}\right),$$

$$E_y(k_x, k_y) = \frac{e}{4\pi^2 c}\left(\frac{e^{-(a/2-y)(f-ik_y)}}{f-ik_y} - \frac{e^{-(a/2+y)(f+ik_y)}}{f+ik_y}\right),$$

$$f = \sqrt{k_x^2 + \eta^2}, \quad \eta^2 = \frac{k^2}{\beta^2\gamma^2}, \tag{2}$$

$$k_x = k \sin\theta \cos\varphi,$$

$$k_y = k \sin\theta \sin\varphi,$$

in which y is the coordinate of the crossing point perpendicular to the slit axis (see Fig. 1) and thus $|y| \le a/2$, while θ and φ are the standard polar angles.

After some mathematical manipulations, the photons number can be written as

$$\frac{dN}{d\Omega} = -\frac{e^2}{8\pi^2\hbar c}\frac{d\lambda}{\lambda}\frac{k^2 e^{-af}}{f^2(f^2+k_y^2)} \times \left\{(f^2+k_x^2)(e^{-2fy}+e^{2fy}) - \frac{2k^2}{\beta^2\gamma^2}\sin(ak_y+\Phi)\right\}, \tag{3}$$

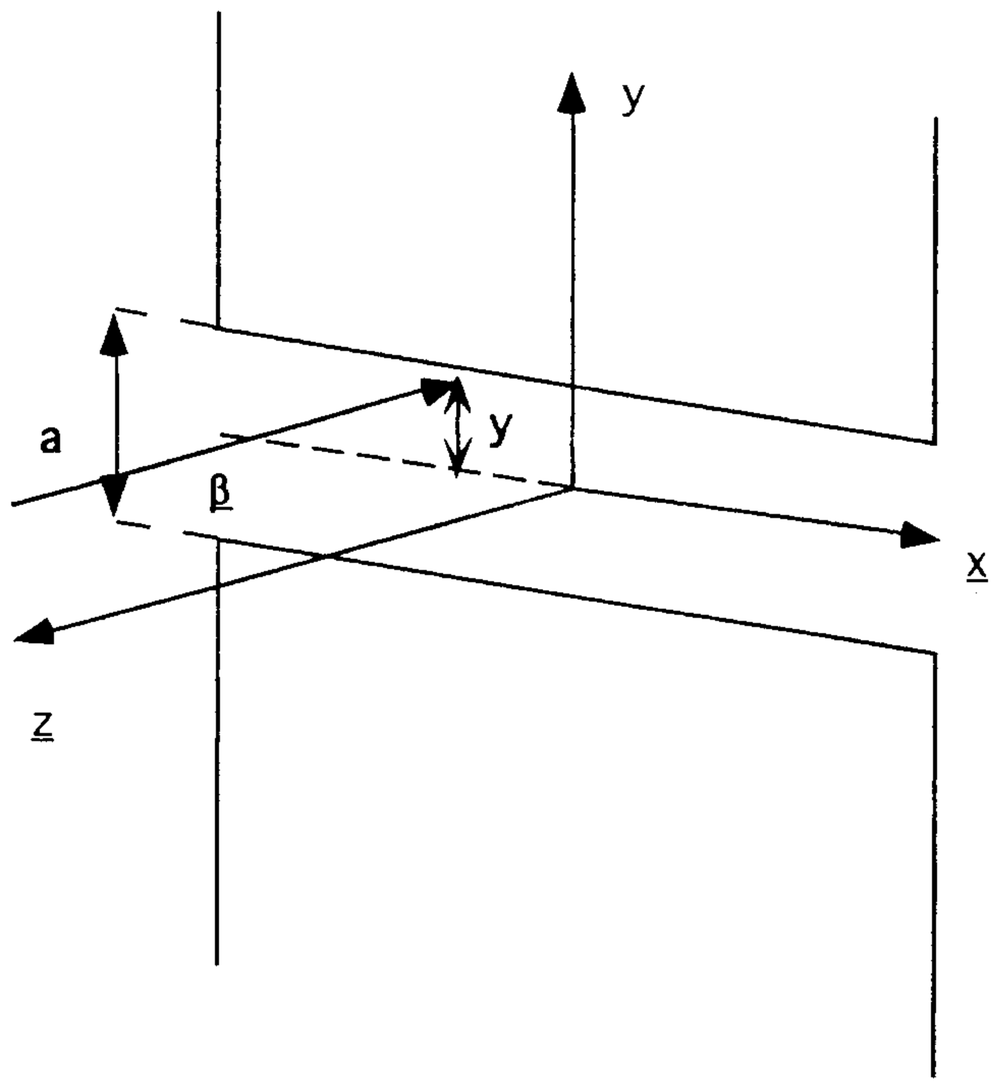

Fig. 1. Slit layout.

with Φ defined by

$$f^2 + k_y^2 = -2fk_y \sin\Phi = (f_2 - k_y^2)\cos\Phi. \tag{4}$$

If the foil carrying the slit is rotated around the vertical y-axis, the same formula (3) applies, under the limiting conditions of a perfect mirror (reflection coefficient equals 1 for all wavelength and all angles) and of $\gamma \gg 1$ (small angles), for the radiation emitted around the direction of specular reflection of the particle velocity. For this reason in the following I will not distinguish between normal or oblique incidence, assuming that the above conditions are always satisfied. In a real device a 45° rotation will allow to extract the radiation through an optical window perpendicular to the beam line and to measure it.

The analysis of formula (3), being $af \ge 2\pi a/\gamma\lambda$, reveals three different behaviours of the radiation pattern as a function of a combination of the main parameters:

(1) for $\gamma\lambda \ll 2\pi a$ the radiation intensity is strongly reduced and no quantitative measurements are possible.

(2) for $\gamma\lambda \gg 2\pi a$ the radiation intensity and angular distribution are very similar to that of transition radiation, with which these coincide in the limit of a going to zero. At energies high enough to satisfy this condition for optical wavelengths, the radiation can be used to make an image of the beam, but at this moment there is no experimental evidence that a resolution better than $\gamma\lambda/2\pi$ can be obtained.

(3) for $\gamma\lambda \sim 2\pi a$ the intensity is somewhat less than that of transition radiation, but enough to make quantitative measurements for the TTF high-charge beam with

up to 6×10^{12} electrons in a macrobunch. In this case interference effects between the two halfplanes of the slit are visible and beam size measurement may be performed in the plane normal to the slit itself.

Before going into the formal derivation of the beam size measurement, I will show a numerical example of the diffraction radiation angular distribution in this regime. The example is based on the parameters given in Table 1.

The intensity and angular distribution of the two polarisation components, with the electric field parallel and normal to the slit, are quite different, the parallel component having an intensity almost one order of magnitude less than the normal one.

The angular distribution of the radiation emitted by an electron crossing the slit in its centre is shown in Figs. 2 and 3 for the two polarisation components.

In the following I will limit the analysis to the normal component, that from (2) and (3) can be written as

$$\frac{dN_\perp}{d\Omega} = -\frac{1}{2}\frac{\alpha}{\lambda^2}\frac{d\lambda}{\lambda}\frac{e^{-af}}{f^2 + k_y^2} \times \{(e^{2yf} + e^{-2yf}) - 2\sin(ak_y + \Phi)\}, \quad (5)$$

where α is the fine structure constant and Φ is defined by Eq. (4).

Table 1
Parameters used in the diffraction radiation calculation

Electron energy	500 MeV
Slit width	1 mm
Wavelength	1 μm

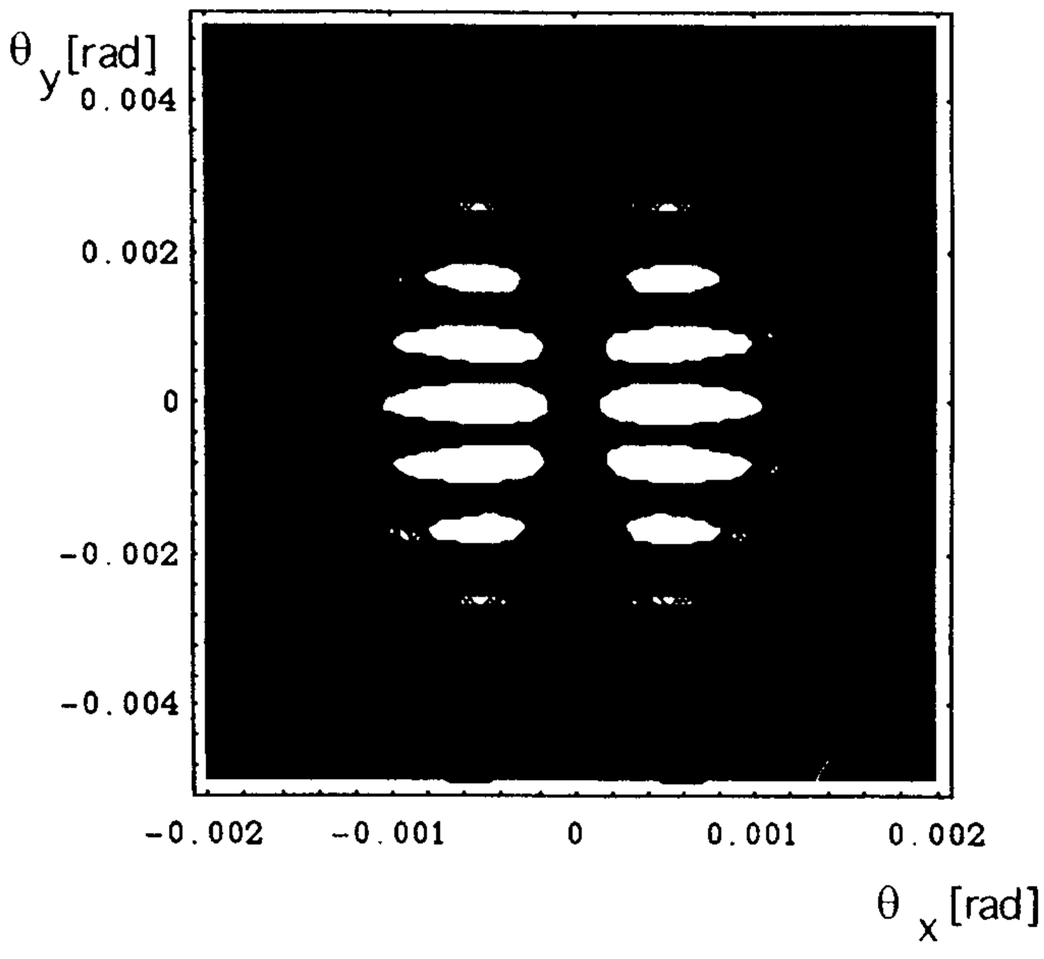

Fig. 2. Angular distribution of 1 μm wavelength diffraction radiation with parallel polarization emitted by a 500 MeV electron crossing a 1 mm slit in its center.

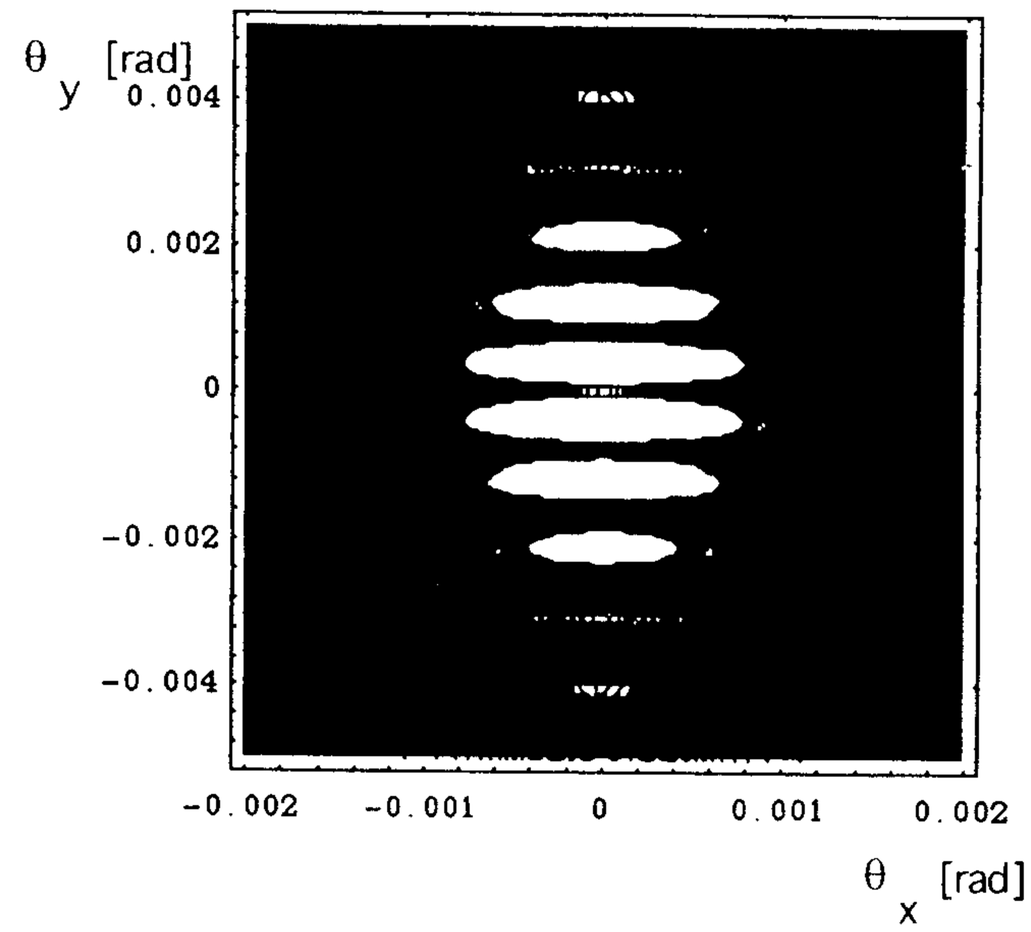

Fig. 3. Angular distribution of 1 μm wavelength diffraction radiation with normal polarization emitted by a 500 MeV electron crossing a 1 mm slit in its center.

3. Diffraction radiation emitted by a gaussian charge distribution

Assuming a beam with a gaussian charge distribution, in the plane normal to the slit, of the form

$$S(x) = \frac{1}{\sqrt{2\pi}\sigma_y} e^{-(y - y_o)^2/2\sigma_y^2},$$

the convolution of (5) with such a distribution gives

$$\frac{dN_\perp}{d\Omega} = -\frac{1}{2}\frac{\alpha}{\lambda^2}\frac{d\lambda}{\lambda}\frac{e^{-af}}{f^2 + k_y^2} \times \{e^{2f^2\sigma_y^2}(e^{2y_o f} + e^{-2y_o f}) - 2\sin(ak_y + \Phi)\}. \quad (6)$$

If $2f^2 y_o^2 \ll 1$ we have

$$e^{2fy_o} + e^{-2fy_o} \cong 2e^{2f^2 y_o^2},$$

and (6) becomes

$$\frac{dN_\perp}{d\Omega} = -\frac{\alpha}{\lambda^2}\frac{d\lambda}{\lambda}\frac{e^{-af}}{f^2 + k_y^2} \times \{e^{2f^2(\sigma_y^2 + y_o^2)} - \sin(ak_y + \Phi)\}. \quad (7)$$

Two consequences can be derived by the inspection of (7):

(1) σ_y and y_o play the same role, that is the intensity emitted by a gaussian beam with standard deviation σ_y crossing the slit in its centre is the same of that emitted by an unidimensional beam (with the same charge) crossing the slit at a position $y_o = \pm \sigma_y$.

(2) The total intensity has a minimum when $y_o = 0$. As has been already shown in Ref. [6], for $a \approx \gamma\lambda$ the sensitivity to the position is strong and the beam can be easily centered on the slit minimising the total intensity.

With the beam centered and for $\theta = 0$, we have

$$\left.\frac{dN_\perp}{d\Omega}\right|_{\theta=0} = -\frac{\alpha}{4\pi^2}\frac{d\lambda}{\lambda}\gamma^2 e^{-2\pi a/\gamma\lambda}\{e^{8\pi^2\sigma_y^2/\gamma^2\lambda^2} - 1\},$$

and from the measurement of the intensity at $\theta = 0$ the beam dimension could be directly derived.

In practice this measurement is impossible due to the extreme difficulty to obtain an absolute calibration of the detector: one must take into account the real dielectric properties of the metallic surface, the absorption and reflection of the vacuum window and of the optical elements, considering also the possible deterioration due to the exposure to high energy radiation, and finally the detector response.

This difficulty can be overcome analysing the whole angular distribution in the plane $\phi = \pm\pi/2$. In this plane, for $y_o = 0$, we have

$$\left.\frac{dN_\perp}{d\Omega}\right|_{\Phi=\pm\pi/2} = -\frac{\alpha}{4\pi^2}\frac{d\lambda}{\lambda}\frac{e^{-2\pi a/\gamma\lambda}}{\theta^2 + 1/\gamma^2} \times\left\{e^{8\pi^2\sigma_y^2/\gamma^2\lambda^2} - \sin\left(\frac{2\pi a\theta}{\lambda} + \Phi\right)\right\}, \quad (8)$$

with $-\pi < \theta < \pi$ ($-\pi < \theta < 0$ for $\phi = -\pi/2$ and $0 \le \theta < \pi$ for $\phi = \pi/2$).

The range in which a significant intensity is present is roughly $|\theta| \le 2/\gamma^2$ as determined by the denominator in (8). If in this range the argument of the sine varies by at least 2π, one or more oscillations will be present in the intensity distribution as function of θ.

A numerical example of the intensity distribution in the yz-plane of the normal polarization radiation emitted with the beam and slit parameters of Table 1 and with $\sigma_y = 0$ is given in Fig. 4, while the same radiation emitted by a beam with a gaussian distribution of standard deviation $\sigma_y = 50$ μm (the nominal value for the TTF FEL beam) is presented in Fig. 5.

A fit of expression (8) on the experimental distribution allows the determination of σ_y, which is the only free parameter, together with a normalisation constant that takes care of the overall detection efficiency.

In fact the oscillating amplitude acts as an auto normalization. This can be more clearly seen in a simplified approach that allows a rapid, but less accurate, beam size determination: let us assume that

$$\left(\frac{2\pi\sigma_y}{\gamma\lambda}\right)^2 \ll 1,$$

from Eq. (8), we can write

$$F(\theta) \equiv \left(\theta^2 + \frac{1}{\gamma^2}\right)\frac{dN_\perp}{d\Omega} = -\frac{\alpha}{4\pi^2}\frac{d\lambda}{\lambda}e^{-2\pi a/\gamma\lambda} \times\left\{2\left(\frac{2\pi\sigma_y}{\gamma\lambda}\right)^2 + \left(1 - \sin\left(\frac{2\pi a\theta}{\lambda} + \Phi\right)\right)\right\}. \quad (9)$$

The behaviour of $F(\theta)$ as function of θ calculated with the same parameters that have been used to derive Fig. 5 is shown in Fig. 6.

It is evident that $F(\theta)$ assumes the minimum values when the sine is 1 and is given by

$$F(\theta)_{\min} = 2A\left(\frac{2\pi\sigma_y}{\gamma\lambda}\right)^2,$$

where A contains all the constant factors, while the maximum values are assumed when the sine is equal to -1:

$$F(\theta)_{\mathrm{Max}} = 2A\left[1 + \left(\frac{2\pi\sigma_y}{\gamma\lambda}\right)^2\right].$$

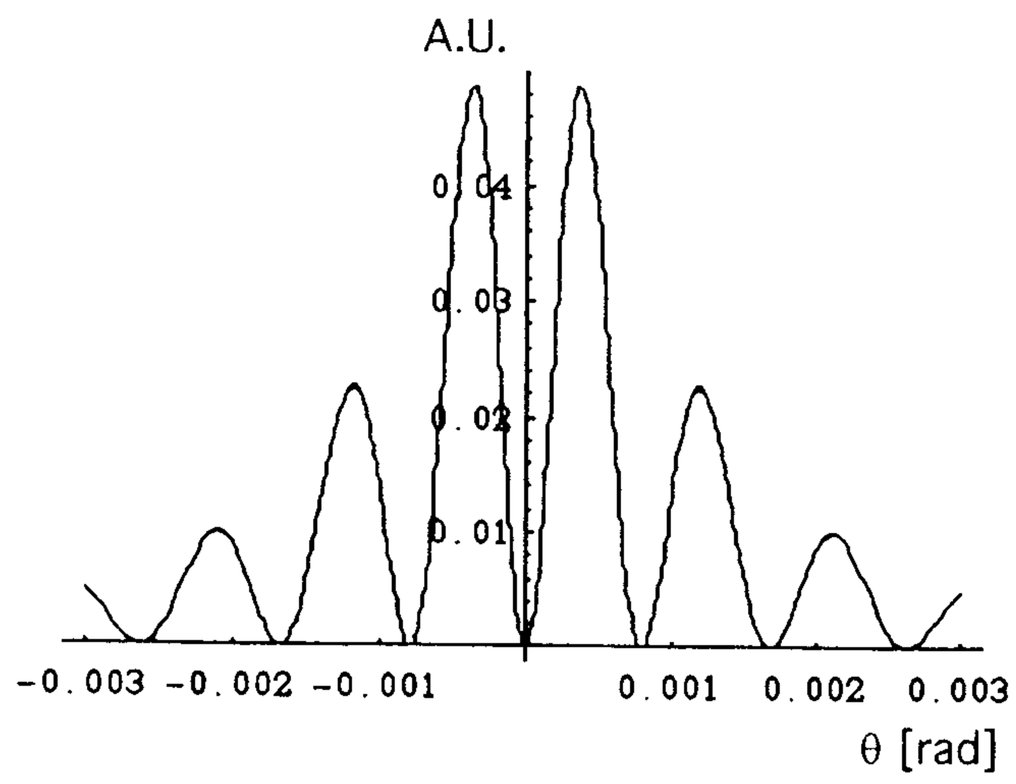

Fig. 4. Radiation angular distribution in the yz-plane from an unidimensional beam crossing the slit center.

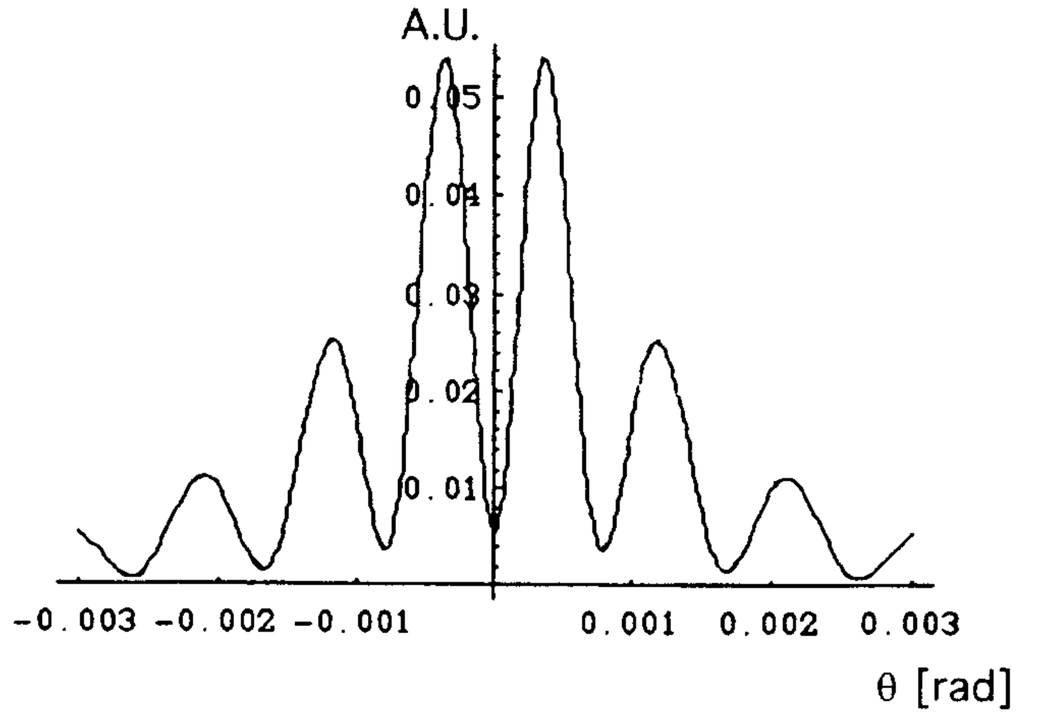

Fig. 5. Radiation angular distribution in the yz-plane from a beam with a gaussian transverse spread of $\sigma_y = 50$ μm crossing the slit center.

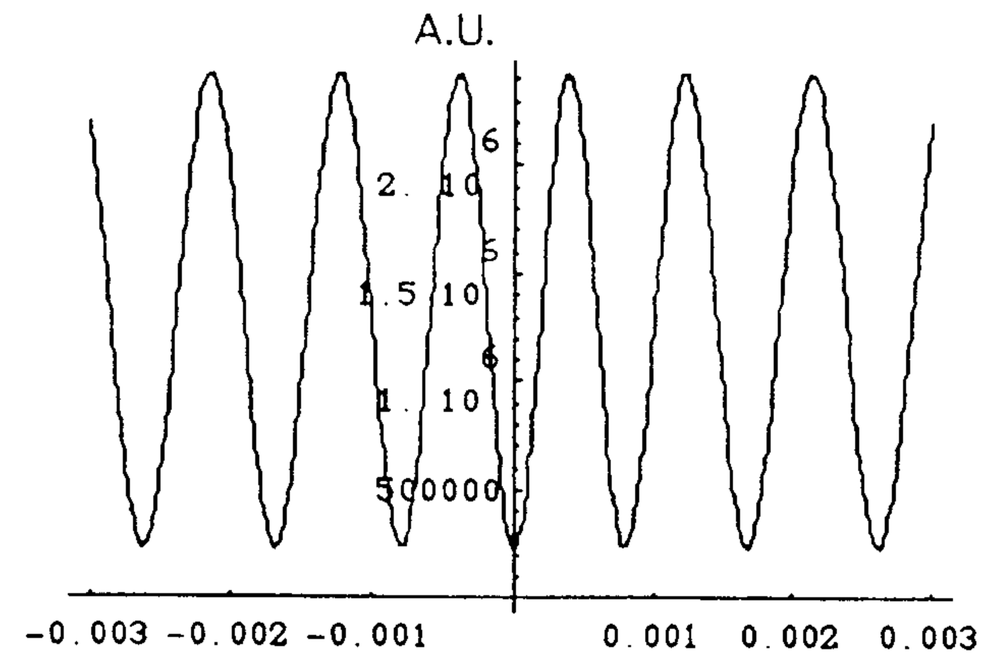

Fig. 6. Behavior of $F(\theta)$ with the parameters used to derive Fig. 5.

Defining

$$R = \frac{F(\theta)_{\min}}{F(\theta)_{\max}},$$

it is easy to see that

$$\frac{2\pi\sigma_y}{\gamma\lambda} = \sqrt{\frac{R}{1-R}},$$

and for $R \ll 1$

$$\sigma_y = \frac{\gamma\lambda}{2\pi}\sqrt{R}. \tag{10}$$

It must be noted that $\gamma\lambda/2\pi$ is the transverse formation zone of the transition radiation, and that some author [6] considers this quantity as the limit in spatial resolution obtainable with this radiation. Being $R < 1$, Eq. (10) gives a beam size inferior to this limit, and derived by a far-field angular distribution, avoiding the problems implied in a near field imaging of a very small beam spot.

With the parameters of Table 1 and assuming $R = 0.01$, a limit value for standard CCD camera with a digital dynamic range of 8 bits, but well within the possibility of high resolution intensified camera, from (10) it results that a beam with a standard deviation as small as $\sigma_y = 16$ μm is measurable.

With a gated intensified camera, provided that enough intensity is produced, it is also possible to select only chosen parts of the macrobunch to verify the stability in time of the beam size.

4. Effects of beam angular spread

Up to now I have considered only a parallel beam. It is evident that the radiation distribution given by Eq. (8), and illustrated in Figs. 4 and 5, is relative to the electron velocity direction, so that a convolution of (8) with a real beam angular distribution in the yz-plane somewhat smoothes out the minimum and maximum values, simulating a larger beam size.

For strongly focalized beams this effect may be dominant and in this case the radiation distribution can be used for a measurement of angular spread. On the other hand, beam size and angular spread give different contribution to the radiation pattern, so that a numerical fit to the experimental data may determine both quantities.

This procedure is highly compute-time consuming, because it is not possible to derive a simple analytical expression for the convolution of (8) with an angular spread distribution, but it is not in the purpose of this work to consider this point. The possibility of a simultaneous measurement of both beam size and angular spread will be investigated in a successive paper. Here I will limit myself to show that for a rather large range of parameters typical of high charge, low emittance beams, a good accuracy measure of beam size can be performed by the detection of diffraction radiation. In fact in these cases a strong focalization is not desired because of the rapid emittance deterioration caused by space charge forces. The TTF FEL beam has a nominal normalized emittance of 2×10^{-6} m rad, and at the entrance of the undulator it is focalized to a transverse size of 50 μm, which corresponds, for a centred phase space ellipse, to an angular divergence of only 20 μrad.

With these values the simplified analysis illustrated in the previous section gives a beam size overestimation of 3%, which becomes of 20% for a much worse emittance of 5×10^{-6} m rad. Even in this extreme case, the beam size can be better measured scaling both the slit width and wavelength. With $a = 0.7$ mm and $\lambda = 700$ nm, i.e. at constant photon flux, the beam size overestimation is reduced to 9%. A larger beam size can be measured without any effect of the angular spread.

The slit width and the detected wavelength must be chosen for each particular experimental situation depending on beam energy, beam size and desired resolution, with the limits given by mechanical accuracy, total photon flux and detector bandwidth. As a general rule, the fewer are the oscillations in the detectable angular range, the less is the influence of angular spread.

5. Effects of the radiation bandwidth

Also the finite bandwidth over which expression (8) must be integrated to be compared with the experimental data has the effect of smoothing out the minimum and maximum values. Although the minimum at $\theta = 0$ is the same for all wavelengths, the other minima and all the maxima are functions of the wavelength. Also in this case

a small number of oscillations helps in reducing the effect, which is fortunately very small for the bandwidth of standard interferential filters.

Infact, with the parameters of Table 1 and a beam size of 50 μm, the integration over an 80 nm bandwidth does not lead to a significant difference in the radiation angular distribution. For a much larger bandwidth, the strong dependence of intensity from wavelength may even result in an underestimation of the beam size if only the first maximum is used for the calculation, as can be seen in Fig. 7 in which the distribution from a monochromatic beam is compared to the one obtained by integrating on a 400 nm bandwidth. The latter has a smoother behaviour, but the first maximum is higher. Using only this value and that of the central minimum (equal for both cases), a beam size value of 46 μm is obtained, that is 8% less than the nominal one.

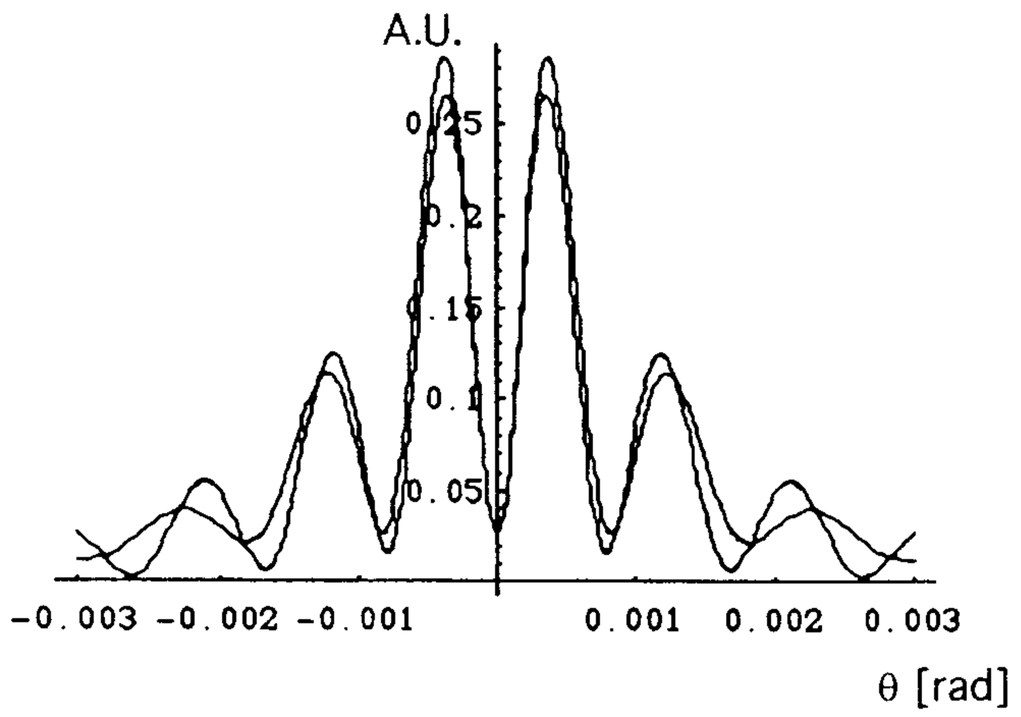

Fig. 7. Comparison of the radiation intensity distribution in the *yz*-plane for a monochromatic and a large bandwidth (400 nm) radiation. The large bandwidth radiation shows a smoother behavior but a higher first maximum.

6. Conclusions

The measurement of angular distribution of diffraction radiation from a slit when interference effects are visible allows the determination of the beam size. A resolution better than the transition radiation transverse formation zone is obtainable.

This method may be used at high energies and short wavelengths for diagnostics of linear collider beams. Its non-intercepting nature allows the determination of beam parameters in operating conditions even with high-charge, low-emittance beams.

References

[1] Ya.S. Derbenev, J. Rossbach, E.L. Saladin, V.D. Shiltsev, Microbunch Radiative Tail–Head Interaction, TESLA-FEL 95-05, Desy, September 1995.
[2] D.A. Edwards (ed.), TESLA Test Facility Linac – Design Report TESLA 95-01 Desy, 1995.
[3] A VUV Free Electron Laser at the TESLA Test Facility at Desy Conceptual Design Report TESLA-FEL 95-03 Desy 1995.
[4] Y.N. Dnestrovskii, D.P. Kostomarov, Sov. Phys. Dokl. 4 (1959) 132.
[5] B.M. Bolotovskii, G.V. Voskresenskii, Sov. Phys. Usp. 9 (1966) 73.
[6] M.J. Moran, B. Chang, Nucl. Instr. and Meth. B 40/41 (1989) 970.
[7] M.L. Ter-Mikaelian, High-Energy Electromagnetic Processes in Condensed Media, Interscience Tracts on Physics and Astronomy No. 29.
[8] M. Castellano, TESLA 96-08, Desy 1996.